Archives of Materials Science and Engineering

Volume 29
Issue 2
February 2008
Pages 97-104

International Scientific Journal
published monthly by the
World Academy of Materials
and Manufacturing Engineering

Mechanical properties of a squeeze cast Mg–Al–Sr alloy

Z. Trojanová [a,*], Z. Drozd [a], P. Lukáč [a], A. Chatey [b]

[a] Department of Physics of Materials, Faculty Mathematics and Physics, Harles University, Prague, Ke Karlovu 5, CZ-121 16 Praha 2, Czech Republic
[b] IPN Grenoble ENSEEG, 6 rue du docteur Mazet, F-38000 Grenoble, France
* Corresponding author: E-mail address: ztrojan@met.mff.cuni.cz

Received 01.03.2007; published in revised form 01.02.2008

ABSTRACT

Purpose: The aim of the present work is to study the influence of temperature on tensile properties of the magnesium alloy AJ50, and to discuss possible hardening and softening mechanisms and thermally activated processes.

Design/methodology/approach: Deformation behaviour of a Mg-Al-Sr magnesium alloy has been studied in tension as well as compression in the temperature interval from room temperature up to 300°C. Stress relaxation tests were performed with the aim to find applied stress components (internal stress and effective stress) and parameters of the thermally activated process/-es.

Findings: The yield stress as well as the maximum stress of the alloy are very sensitive to the testing temperature. The work hardening coefficient $\Theta=d\sigma/d\varepsilon$ decreases with increasing stress and temperature. Performed analysis of the Θ-σ plots determined the hardening and softening mechanisms operating during the deformation. The internal stress decreses with increasin temperature, while the effective stress component increases.

Practical implications: Estimated values of the activation volume as well as the activation energy indicate that the main thermally activated process is connected with the rapid decrease of the internal stress.

Originality/value: An analysis showed that the main hardening process is the storage of dislocations at impenetrable obstacles. The activation volume values indicate that the main thermally activated process is connected with recovery process.

Keywords: Mechanical properties; Magnesium alloy; Stress relaxation; Hardening; Thermal activation

PROPERTIES

1. Introduction

Most commercial magnesium alloys (e.g. AZ and AM series) exhibit a relative high specific strength (the strength/density ratio) at room temperature but poor mechanical properties at elevated temperatures [1-6]. The mechanical properties of magnesium alloys are widely influenced by alloying elements and thermal treatments. The strength of cast magnesium alloys is obtained by one or more of the well known hardening mechanisms: solid solution hardening, grain size refinement or Hall-Petch hardening, precipitation strengthening and dispersion hardening. Special industrial applications require improvement of the high temperature properties. For these elevated temperatures applications, alloys containing rare earth elements have been developed. New Mg-Al-Sr alloys are being developed with the aim to find cast alloys with good creep resistance and good strength alloys and replace expensive rare earth alloying elements with some cheaper one. Pekguleryuz [7] reported that Mg-Al-Sr alloys show different microstructures based on the Sr/Al ratio. For Sr/Al ratio below about 0.3, only Al_4Sr intermetallic phase is present as the second phase in the structure. When the Sr/Al ratio is higher, a second intermetallic phase, a new, ternary Mg-Al-Sr compound, is observed. When the Sr/Al ratio is very low, there is insufficient amount of Sr to bind all Al atoms and the excess Al would form the $Mg_{17}Al_{12}$ phase. These conclusions were

confirmed by Parvez et al. [8] who investigated 22 alloys from the Mg-Al-Sr system. They have reported that Al_4Sr and Mg solid solution are the dominating phases. They found also a new $Al_3Mg_{13}Sr$ phase. Kunst et al. [9] studied creep behaviour of three AJ62 alloys with the different Al/Sr ratio (from 2.0 to 2.7) in a wide range of temperatures and stresses. The microstructure of the AJ62 alloy is characterised by a primary α-Mg solid solutions with globular morphology and secondary phases in between these regions. The morphology of the second phase is lamellar eutectics, which consists of Al_4Sr and secondary α-Mg lamellae. Lamellar eutectic has been also reported in [10].

There is very limited information about the mechanical properties of Mg-Al-Sr alloys and therefore it is important to investigate mechanical properties at different temperatures and to estimate the mechanisms responsible for the deformation behaviour of Mg-Al-Sr alloys at elevated temperatures.

The aim of the present work is to study the influence of temperature on tensile properties of the magnesium alloy AJ50, and to discuss possible hardening and softening mechanisms and thermally activated processes.

2. Experimental procedure

The AJ50 magnesium alloy (nominal composition in w%: 5Al-0.6Sr-balance Mg) used in this study was prepared by the squeeze cast technique [19]. Samples were deformed in an Instron machine over the temperature range from 23 to 300 °C. Cylindrical specimens with a diameter of 5 mm and a length of 27 mm were deformed in tension tests at an initial strain rate of 3.1 $x10^{-5}$ s^{-1}. Samples for compression tests with dimensions of 5x5x10 mm^3 were deformed at an initial strain rate of $8x10^{-5}$ s^{-1}. The temperature in the furnace was maintained with an accuracy of ±1°C. Sequential stress relaxation (SR) tests were performed at increasing stress (strain) along a stress-strain curve. Duration of the SR was 300 s. The microstructure of samples was observed by the light optical microscopy (LOM).

3. Experimental results

Figure 1 shows optical micrograph of the as cast alloy. The primary Mg grains are surrounded by the interconnected network of the grain boundary phase.

This phase is formed during solidification process and it has lamellar type morphology. The γ phase ($Mg_{17}Al_{12}$) is also visible. Al_4Sr phase with lamellar eutectic morphology is similar to that found in [8] for alloy with similar composition.

The true stress-true strain curves obtained in tension tests at various temperatures are shown in Figure 2. It can be seen low ductility of the alloy at lower temperatures, while at higher temperatures the ductility increases up to 20-25%.

The flow curves obtained in compression tests are introduced in Figure 3. Samples were deformed either to failure or the tests performed at temperatures higher than 100 °C were interrupted at a predetermined strain.

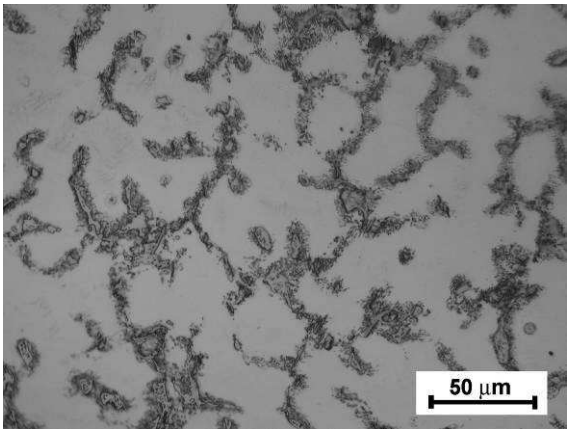

Fig. 1. LOM micrograph of as cast alloy

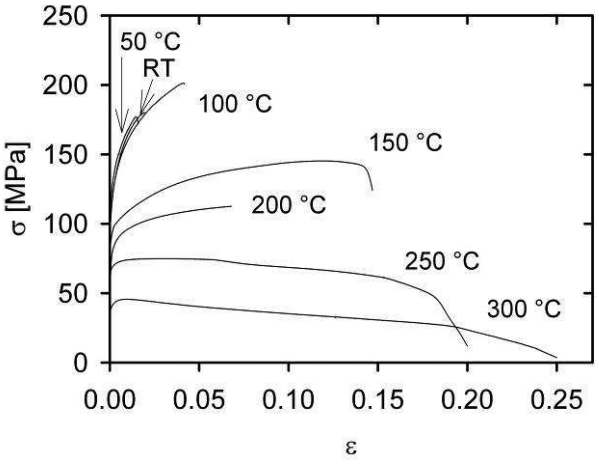

Fig. 2. Stress strain curves obtained for various temperatures obtained in tension

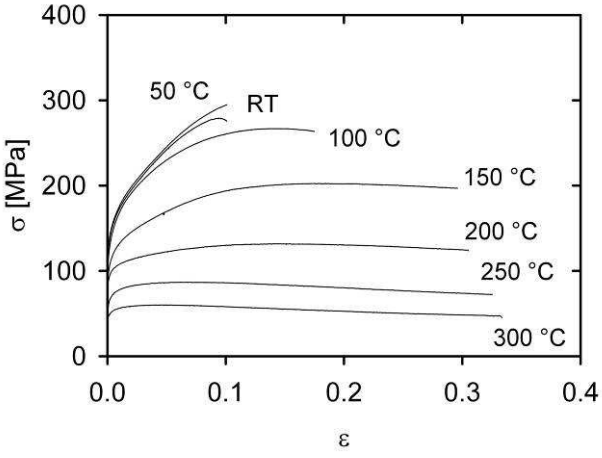

Fig. 3. Stress strain curves obtained for various temperatures in compression

Figure 4 shows the temperature dependence of the yield stress as well as the maximum stress for both types of tests. While the values of the yield stress are practically the same for tension and compression, the values of the maximum stress are higher in compression tests. The characteristic stresses decrease with increasing temperature for T > 50 °C. The small local maximum in the temperature dependence in the vicinity of 50 °C was observed in several Mg alloys and composites [2,11] and it is caused by a dynamic age hardening.

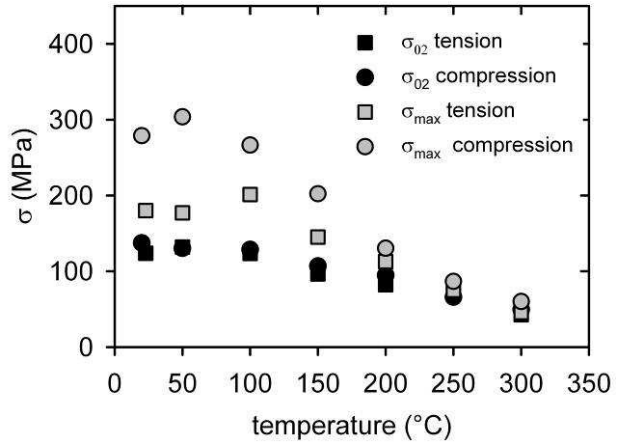

Fig. 4. Temperature dependence of yield stress and maximum stress

In a stress relaxation test, the specimen is deformed to a certain stress σ_0 and then the machine is stopped and the stress is allowed to relax. The stress decreases with the time t. The specimen can be again reloaded and deformed to a higher stress (strain) and the stress relaxation test may be repeated. The sequence of the stress relaxation curves i.e. a decrease of the stress with time, when the deformation apparatus was stopped, obtained at 100 °C in compression is given in Figure 5 (For the clarity only curves obtained up to the maximum stress were depicted.)

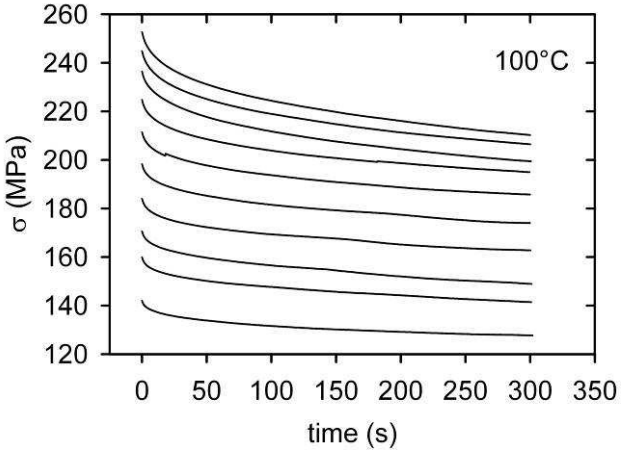

Fig. 5. Sequence of the stress relaxation curves obtained at 100°C in compression

4. Discussion

4.1. Strain hardening

It is widely accepted that the resolved shear stress τ necessary for the dislocation motion in the slip plane can be divided into two components:

$$\tau = \tau_i + \tau^*, \tag{1}$$

where τ_i is the (internal) athermal contribution to the stress, resulting from long-range internal stresses impeding the plastic flow;

$$\tau_i = \alpha_1 G b \rho_t^{1/2}, \tag{2}$$

where G is the shear modulus, α_1 is a constant describing interaction between dislocations, b is the Burgers vector of dislocations and ρ_t is the total dislocation density. The effective shear stress τ* acts on dislocations during their thermally activated motion when they overcome short range obstacles. The dislocation velocity (the plastic shear strain rate) is controlled by obstacles (their strength, density) and it depends on temperature and the effective shear stress. In polycrystalline materials, the resolved shear stress τ and its components are related to the applied stress σ and its corresponding components by the Taylor orientation factor ψ: $\sigma = \psi\tau$. The flow stress, σ, of ductile metals depends on the average dislocation density, ρ_t, as $\sigma \propto \sqrt{\rho_t}$ [13]. The dislocation structure evolves with plastic deformation. Dislocations stored at the obstacles contribute to hardening while processes such as cross slip and climb of dislocations contribute to softening. Dislocations after cross slip and/or climb may annihilate, which causes a decrease in the work hardening rate $\Theta = (\partial\sigma/\partial\varepsilon)_{\dot{\varepsilon},T}$ (where ε is the true plastic strain and T is the temperature), usually observed at large applied stresses and strains.

The stress dependence of the work hardening rate in metallic materials has been modelled by a number of authors. Lukáč and Balík [13] divide their evolution equation of dislocation density into two hardening and two softening components. They assume that the hardening occurs due to the multiplication of dislocations at both impenetrable obstacles and forest dislocations. Annihilation of dislocations, due to cross slip and dislocation climb, is considered as the dominant softening process. The overall evolution of the dislocation density with strain thus can be described as

$$\frac{\partial\rho}{\partial\varepsilon} = K_1 + K_2\rho^{1/2} - K_3\rho - K_4\rho^2, \tag{4}$$

where $K_1 = 1/bs$, s is the spacing between impenetrable obstacles, K_2 is a coefficient of the dislocation multiplication intensity due to interaction with forest dislocations, K_3 and K_4 are coefficients of dislocation recovery intensity due to cross slip and climb of dislocations, respectively. Both coefficients K_3 and K_4

depend on temperature and strain rate. The stress dependence of the work hardening rate for polycrystals can thus be written in the form:

$$\Theta = A/(\sigma - \sigma_y) + B - C(\sigma - \sigma_y) - D(\sigma - \sigma_y)^3, \quad (5)$$

where the parameter A is connected with the interaction of dislocations with the non-dislocation obstacles and is expected to increase with increased solute content or the presence of precipitates of second phase particles; the parameter B relates to the work hardening due to the interaction with forest dislocations; the parameter C relates to recovery due to cross slip; the parameter D is connected with climb of dislocations and σ_y is the applied yield stress. Both C and D are related to thermally activated processes and are expected to increase with temperature.

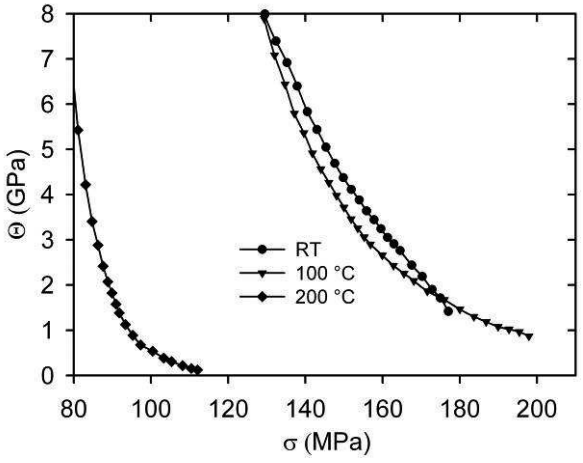

Fig. 6. Stress dependence of work hardening coefficient obtained for three temperatures in tension

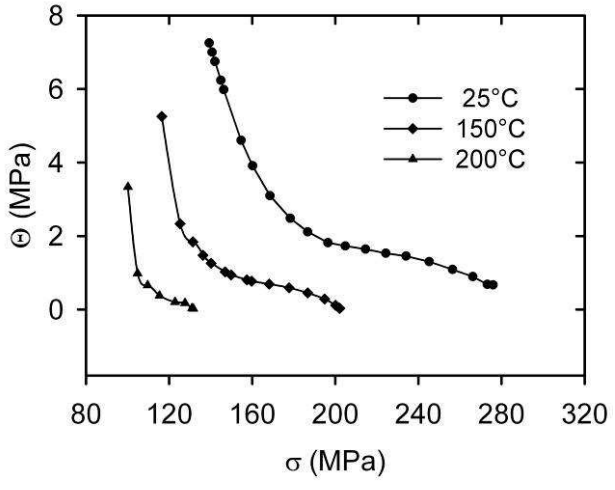

Fig. 7. Stress dependence of work hardening coefficient obtained for three temperatures in compression

The strain hardening coefficient, Θ, calculated from the experimental tensile and compression curves of Figures 2, 3 are introduced in Figures 6,7 for selected temperatures.

Experimental values of Θ were fitted according to eq. (5) and the model parameters have been estimated. An analysis of the work hardening rate obtained in tension gives very high values of the A parameter. Other parameters are not significant for the fit at room temperature. It means that the non-dislocation obstacles are the most important for the development of the dislocation substructure. Al_4Sr and $Mg_{17}Al_{12}$ are incoherent and they have the highest influence on the hardening that is realised by storage of dislocations on these obstacles. The stress dependence of the work hardening rate of samples deformed in compression is shown in Figure 7. Similar analysis of the work hardening rate according to eq. (5) gives the values of the model parameters introduced in Table 1. It should be mentioned that the Lukáč and Balík model describes reasonably the experimentally estimated stress dependence of the work hardening rate only at temperatures up to 200 °C. From the Table 1 it follows that the main dislocation obstacles remain the impenetrable obstacles.

Table 1.
Parameters of the tested model

	25°C	50°C	100°C	150°C	200°C
σ_y (MPa)	124.0	116.0	108.0	94.4	88
A (MPa^2)	105000	125000	176000	753000	15900
B (MPa)	742	630	454	20	5.7
C	3.07	2.98	8.14	4.70	7.47
D (MPa^{-2})	4.94e-9	2.43e-8	4.81e-8	2.00e-4	8.46e-9
σ_{02} (MPa)	123.8	132	123.5	96.5	82.2

The development of the dislocation density increases the storage probability of dislocations. With increasing temperature the storage probability should decrease. This could cause the temperature decrease in the parameter B that is really observed. The parameter C increases with temperature, which indicates that cross slip becomes a significant recovery process at higher temperatures. The parameter *D* increases with increasing temperature, which is expected in the case of climb. Above 200°C the model does not describe the experimental curves satisfactory. A decrease in the forest dislocation density (the density of dislocations in non-basal planes) can be expected with increasing temperature. The activity of the pyramidal slip system, with (**c** + **a**) dislocations, increases with increasing temperature. The (**c** + **a**) dislocations may annihilate after double cross slip. This leads to the dislocation density decrease. The mean free path of dislocations and therefore the storage distance will increase.

4.2. Stress relaxation

Components of the applied stress (σ_i, σ^*) were estimated using Li's method [14]. The SR curves were fitted to the power

law function in the form:, where a, t_0 and m are fitting parameters. A part of the true stress-true strain curve measured in compression at 25 ºC with points indicating the stresses at which the SR tests were performed is shown in Figure 8. Blank circles and full circles depict the internal stress σ_i, and the effective stress, respectively. It is obvious that the internal stress σ_i is a substantial contribution to the applied stress σ_{ap}.

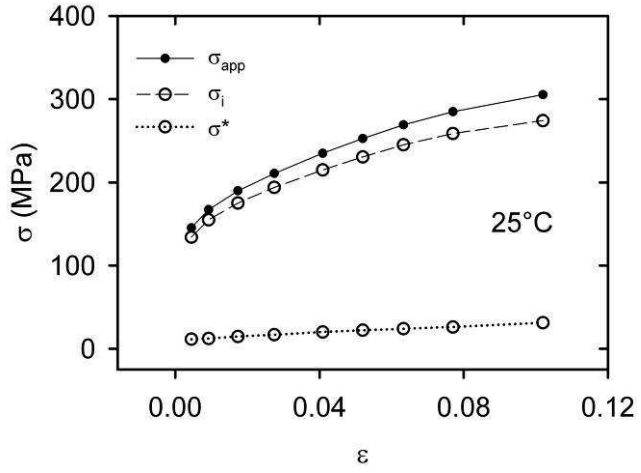

Fig. 8. A part of the true stress-true strain curve obtained at room temperature in compression. Components of the applied stress are depicted. The points on the curve indicate the stresses at which the SR tests were performed

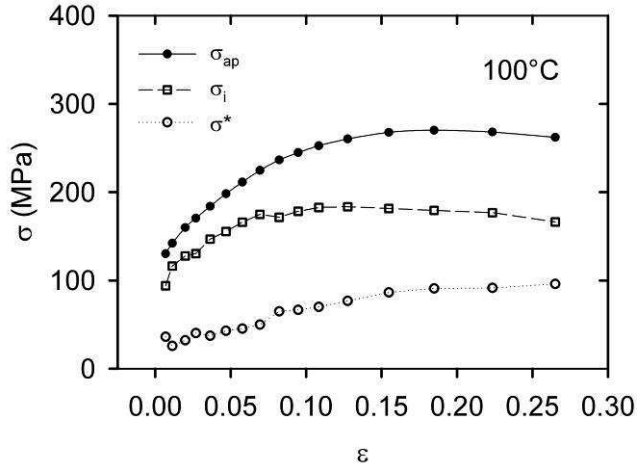

Fig. 9. A part of the true stress-true strain curve obtained at 100°C. Components of the applied stress are depicted. The points on the curve indicate the stresses at which the SR tests were performed

Similar curves estimated for 100 °C are shown in Figure 9. The effective stress component increases with increasing strain while the internal stress increases to the maximum and then decreases with increasing strain. Figure 10 shows the stress dependences of σ_i as well as σ^* estimated in tension for various temperatures. Because of low ductility of samples only several SR tests could be performed during the tensile deformation. The ratio of the effective stress to the applied stress increases with increasing temperature. Components of the internal stress (full points) and the effective stress (empty points) estimated in compression tests are plotted against strain in Figure 11.

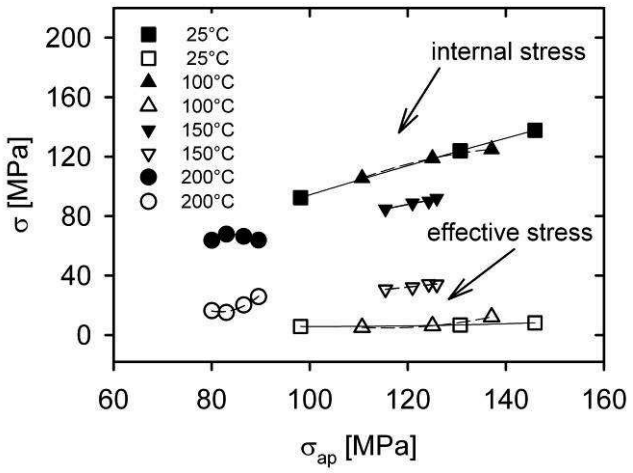

Fig. 10. Components of the internal stress and effective stress depending on the applied stress estimated for various temperatures in tension

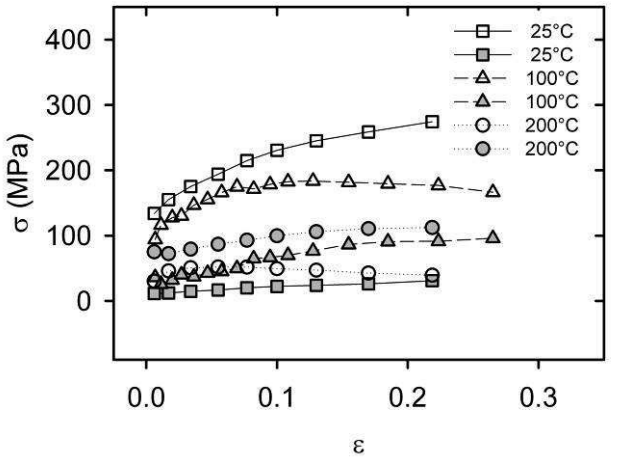

Fig. 11. Components of the internal stress and effective stress depending on the applied stress estimated for various temperatures in compression

It is important to mention that the values of the internal stress at 200 °C are lower than those of the effective stress. This indicates a decrease of the total dislocation density and the occurrence of softening process/-es.

4.3. Thermal activation

The time derivative $\dot{\sigma} = d\sigma/dt$ is the stress relaxation rate and $\sigma = \sigma(t)$ is the flow stress at time t during the SR. Stress relaxation tests are very often analysed under the assumption that the stress relaxation rate is proportional to the strain rate $\dot{\varepsilon}$ according to as:

$$\dot{\varepsilon} = -\dot{\sigma}/M \tag{6}$$

where M is the combined modulus of the specimen – machine set. Considering that the SR is thermally activated dislocation motion through the field of local obstacles, the mean velocity of dislocations is connected with the strain rate by the Orowan equation

$$\dot{\varepsilon} = (1/\psi)\rho\, b\, v \tag{7}$$

where v is the mean dislocation velocity. It is obvious that the stress dependence of $\dot{\varepsilon}$ is done by the stress dependence of ρ and v. At finite temperature, the obstacles can be overcome with the help of thermal fluctuation. Therefore, the dislocations are able to move even if the force on dislocations is lower than the force exerted by the obstacles; the additional energy is supplied by thermal fluctuations. If a single process is controlling the rate of dislocation glide, the plastic strain rate $\dot{\varepsilon}$ can be expressed as:

$$\dot{\varepsilon} = \dot{\varepsilon}_0 \exp\left[-\frac{\Delta G(\sigma^*)}{kT}\right], \tag{8}$$

where $\dot{\varepsilon}_0$ is a pre-exponential factor containing the dislocation density, the average area covered by the dislocations in every activation act, the Burgers vector, the vibration frequency, and the geometric factor. $\Delta G(\sigma^*)$ is the change of Gibbs free enthalpy depending on the effective stress σ^*, k is the Boltzmann constant and T is the absolute temperature. The stress dependence of the Gibbs free enthalpy my be expressed by a simple relation

$$\Delta G(\sigma^*) = \Delta G_0 - V\sigma^*, \tag{9}$$

where ΔG_0 is the Gibbs free energy (called the barrier activation energy) in the absence of stress and V is the activation volume. The nature and the distribution of obstacles determine the activation parameters (the activation energy and the activation volume). For a given arrangement of obstacles in a material, the thermally activated process determines the temperature and strain rate dependence of the flow stress. The activation energy ΔG_0 and the activation volume V are needed to identify the thermally activated mechanism.

Combining (6), (8) and (9), we have

$$-\dot{\sigma} = M\,\dot{\varepsilon}_0 \exp\left[-\frac{\Delta G_0 - V\sigma^*}{kT}\right]. \tag{10}$$

Taking the logarithm of this equation we get

$$\ln(-\dot{\sigma}) = \ln(M\dot{\varepsilon}_0) - \frac{\Delta G_0}{kT} + \frac{V\sigma^*}{kT}. \tag{11}$$

Integration of (11) results to the known Feltham equation [15]

$$\Delta\sigma(t) = \sigma(0) - \sigma(t) = \alpha\ln(\beta t+1), \tag{12}$$

where $\sigma(0)$ is the stress at the beginning of stress relaxation at time t = 0,

$$\alpha = \frac{kT}{V}, \tag{13}$$

$$\beta = \frac{M\dot{\varepsilon}_0 V}{kT}\exp\left[-\frac{\Delta G_0 - V\sigma^*(0)}{kT}\right] = \frac{M\dot{\varepsilon}(0)}{\alpha}, \tag{14}$$

where $\dot{\varepsilon}(0)$ the plastic strain rate at the beginning of the relaxation.

The activation volumes V_{app} for AJ50 magnesium alloy polycrystals were estimated using equations (12) and (13). As usual, the values of V divided by b^3 for samples deformed in compression are plotted against the applied stress for three testing temperatures in Figure 12.

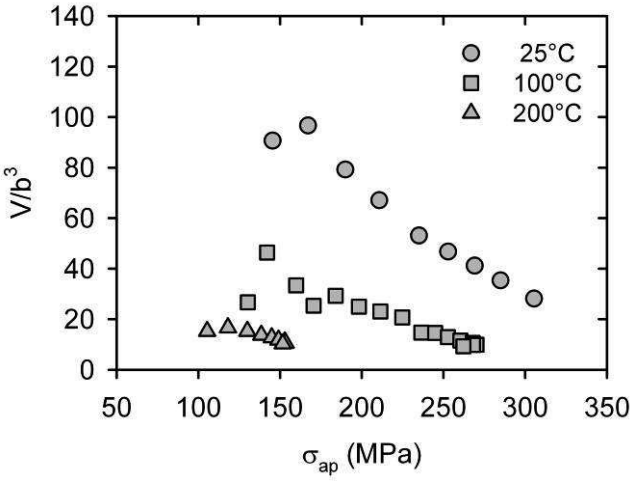

Fig. 12. Activation volume in b^3 estimated in compression depending on the applied stress for three temperatures

It can be seen that the activation volumes decrease with applied stress for all temperatures measured. If the activation volumes for all temperatures are plotted against the effective stress σ*, the values appear to lie on one line - "master curve" (Figure 13 for tension and Figure 14 for compression). Kocks et al. [16] suggested an empirical equation between the Gibbs enthalpy ΔG and the effective stress σ* in the following form:

$$\Delta G = \Delta G_0 \left[1 - \left(\frac{\sigma^*}{\sigma_0^*} \right)^p \right]^q , \quad (15)$$

where ΔG_0 and σ_0^* are Gibbs enthalpy and the effective stress at 0 K. For the effective stress it follows:

$$\sigma^* = \sigma_0^* \left[1 - \left(\frac{kT}{\Delta G_0} \ln \frac{\dot{\varepsilon}_0}{\dot{\varepsilon}} \right)^{1/q} \right]^{1/p} , \quad (16)$$

where p and q are phenomenological parameters reflecting the shape of a resistance obstacle profile.

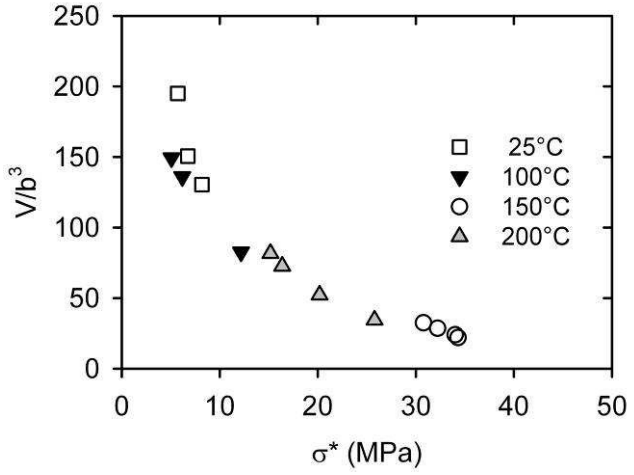

Fig. 13. The plot of the activation volume in b^3 against the thermal stress estimated for various temperatures in tension

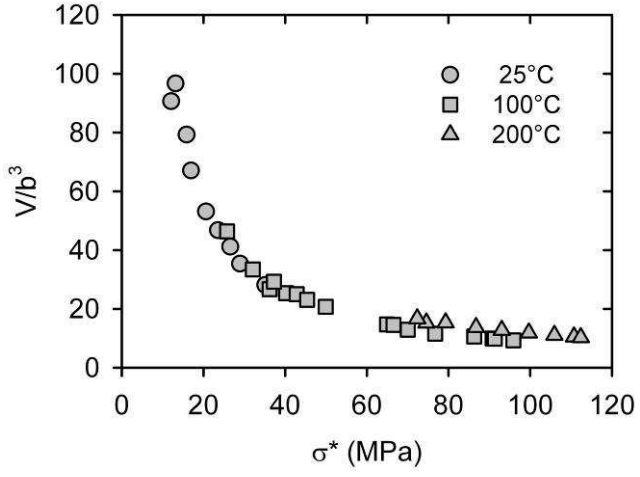

Fig. 14. The plot of the activation volume in b^3 against the thermal stress estimated for various temperatures in compression

The possible ranges of values p and q are limited by the conditions $0 < p \leq 1$ and $1 \leq q \leq 2$. Ono [17], suggested that Equation (16) with p = 1/2, q = 3/2 describes a barrier shape profile that fits many predicted barrier shapes. Thermodynamics generally defines the activation volume as

$$V = -\left(\frac{d\Delta G}{d\sigma^*} \right)_T = kT \left(\frac{d \ln \dot{\varepsilon}}{d\sigma^*} \right) = kT \left(\frac{d \ln(-\dot{\sigma})}{d\sigma^*} \right)_T . \quad (17)$$

Equation (17) can be rewritten as

$$V = \frac{\Delta G_0 pq}{\sigma_0^*} \left[1 - \left(\frac{\sigma^*}{\sigma_0^*} \right)^p \right]^{q-1} \left(\frac{\sigma^*}{\sigma_0^*} \right)^{p-1} . \quad (18)$$

The values of the activation volume should lie at the curve given by the equation (19). Using binominal expansion in (19), the activation volume should depend on the effective stress $V_{app} \propto (\sigma^*)^{-n}$. All data estimated for the activation volume (tension, compression, at all temperatures studied) are introduced in Figure 15 in the bilogarithmic scale.

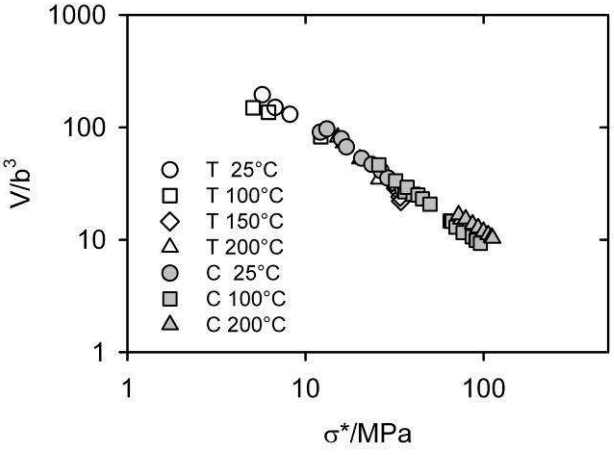

Fig. 15. Activation volume data estimated in tension (empty symbols) and compression (full symbols) for various temperatures

It can be seen that all values lie approximately at one straight line with the slope -0.9. Generally, the values of the power exponent found in the literature vary from -0.5 to -1 [17]. The activation enthalpy $\Delta H = \Delta G - T\Delta S$ (ΔS is the entropy) is done by

$$\Delta H = -TV \frac{d\sigma}{dT} . \quad (20)$$

The differential coefficient $d\sigma/dT$ was estimated from the temperature dependence of the yield stress in the temperature range from 100 to 200 °C. The activation enthalpy calculated according to (20) for 100 °C gives (1.00 ± 0.05) eV. Similar value of 0.95 eV has been reported for Mg in creep experiments at 400 K [18]. The values of the activation volume and the activation

enthalpy may help to identify thermally activated process. The dislocation–dislocation interaction mechanism has an activation volume ranging between 10^2–10^4 b^3, with the activation volume and enthalpy varying with strain. A rapid decrease in the internal stress with temperature (see Figure 7) indicates that softening is connected with dynamic recovery.

5. Conclusions

The deformation behaviour of the AJ50 magnesium alloy has been studied in tension as well as in compression over the temperature range from room temperature to 300 °C.

- An analysis of the hardening and softening processes showed that the main hardening process is the storage of dislocations at impenetrable obstacles. These obstacles are Al_4Sr and $Mg_{17}Al_{12}$ incoherent precipitates.
- The internal stress estimated using stress relaxation tests decreases with increasing testing temperature. It is due to recovery processes that play significant role during deformation at elevated temperatures.
- The activation volume depends on the thermal stress so that all values lie at the master curve $V_{app} \propto (\sigma^*)^{-n}$.
- The estimated activation energy and values of the activation volume indicates that the main thermally activated process is very probably the glide of dislocations in the non-compact planes.

Acknowledgements

This work is a part of the research project 1M 2560471601 “Eco-centre for Applied Research of Non-ferrous Metals” financed by the Ministry of Education, Youth and Sports of the Czech Republic.Republic. Financial support of the Grant Agency of the Academy of Sciences of the Czech Republic by the Grant No. A201120603 is also acknowledged.

References

[1] L. Čížek, M. Greger , L. Pawlica , L.A. Dobrzański and T. Tański, Study of selected properties of magnesium alloy AZ91 after heat treatment and forming, Journal of Materials Processing Technology 157-158 (2003) 466-471.

[2] Z. Trojanová and P. Lukáč, Compressive deformation behaviour of magnesium alloys, Journal of Materials Processing Technology 162-163 (2005) 416-421.

[3] M. S. Yong and A. J. Clegg, Process optimisation for a squeeze cast magnesium alloy, Journal of Materials Processing Technology 145 (2004) 134-141.

[4] M. Pahutová, V. Sklenička, K. Kuchařová, M. Svoboda, Creep resistance of magnesium alloys and their composites, International Journal of Materials and Product Technology 18 (2003) 116-140.

[5] A. Kiełbus, Structure and Machanical Properties of casting MSR-B magnesium alloy, Journal of Achievements in Materials and Manufacturing Engineering 18 (2006) 131-134.

[6] A. Kiełbus, Microstructure of AE44 magnesium alloy before and after hot chamber die casting, Journal of Achievements in Materials and Manufacturing Engineering 20 (2007) 459-462.

[7] M. Pekguleryuz, Creep resistant magnesium alloys for powertrain applications, Magnesium Alloys and Their Applications (Ed. K.U. Kainer), DGM, Willey-VCH 2003, 65-85.

[8] M. A. Parvez, M. Medraj, E. Essadiqi, A. Muntasar, G. Dénès, Experimental study of the ternary magnesium–aluminium–strontium system, Journal of Alloys and Compounds 402 (2005) 170-185.

[9] M. Kunst, A. Fischerworring-Bunk, U. Glatzel, G.L’Espérance, P. Plamodon, E. Baril, P. Labelle, Creep deformation mechanisms of AJ (Mg-Al-Sr) alloys. Proceedings of International Symposium on Magnesium Technology in the Global Age. Canad. Institute of Mining, Metallurgy and Petroleum, Montréal, Canada 2006, 647-661.

[10] E. Baril. P. Labelle, M.O. Pekguleryuz, Elevated temperature Mg-Al-Sr, creep resistance, mechanical properties, and microstructure, Journal of the Minerals, Metals and Materials (JOM) 55 (2003) 34-39.

[11] Z. Drozd, Z. Trojanová, V. Gärtnerová, Deformation behaviour of Mg-Li-Al alloys at room and elevated temperatures, Magnesium Alloys and Their Applications, Ed. K.U. Kainer, DGM, Willey 2003, 122-127.

[12] U.F. Kocks, Laws for work hardening and low temperature creep, Journal of Engineering Materials and Technology 98 (1976) 76-85.

[13] P. Lukáč, J. Balík, Kinetics of plastic deformation, Key Engineering Materials, 97-98 (1994) 307-322.

[14] J.C.M. Li, Dislocation Dynamics in Deformation and Recovery, Canadian Journal of Applied Physics 45 (1967) 493-509.

[15] P. Feltham, Stress relaxation in magnesium at low temperatures, Physica Status Solidi 3 1963, 1340-1346.

[16] U.F. Kocks, A.S. Argon, M.F. Ashby, Thermodynamics and kinetics of slip, Progress in Materials Science 19 (1975) 1-288.

[17] K. Ono, Temperature dependence of dispersed barrier hardening, Journal of Applied Physics 39 (1968) 1803-1806.

[18] S.S. Vagarali, T.G. Langdon: Deformation mechanisms in HCP metals at elevated temperatures.1. Creep behaviour of Magnesium, Acta Metallurgica 29 (1981) 1969-1982.

[19] Z. Trojanová, Z. Drozd, P. Lukáč, Compressive behaviour of a squeeze cast AJ50 magnesium alloy, Journal of Achievements in Materials and Manufacturing Engineering 22/2 (2007) 45-48.